fractal and fractional

Article

Correlating Morphology and Multifractal Spatial Patterns of the Leaf Surface Architecture of *Anacardium occidentale* L.

Glenda Quaresma Ramos [1], Robert Saraiva Matos [2,3], Abhijeet Das [4], Sanjeev Kumar [4], Ştefan Ţălu [5,*] and Henrique Duarte da Fonseca Filho [6]

1 Morphology Department, Institute of Biological Sciences, Federal University of Amazonas-UFAM, Manaus 69077-000, Brazil; gq.ramos@hotmail.com
2 Physics Department, Amazonian Materials Group, Federal University of Amapá-UNIFAP, Macapá 68903-419, Brazil; amazonianmaterialsgroup@gmail.com
3 Postgraduate Program in Materials Science and Engineering, Federal University of Sergipe-UFS, São Cristóvão 49100-000, Brazil
4 Centre for Advance Research, Department of Physics, Rajiv Gandhi University, Rono Hills 791112, India; abhijeet.das@rgu.ac.in (A.D.); sanjeev.kumar@rgu.ac.in (S.K.)
5 The Directorate of Research, Development and Innovation Management (DMCDI), Technical University of Cluj-Napoca, Constantin Daicoviciu St., No. 15, 400020 Cluj-Napoca, Romania
6 Physics Department, Laboratory of Synthesis of Nanomaterials and Nanoscopy, Federal University of Amazonas-UFAM, Manaus 69077-000, Brazil; hdffilho@ufam.edu.br
* Correspondence: stefan.talu@auto.utcluj.ro

Abstract: Plant leaf surfaces can contain interesting, reproducible spatial patterns that can be used for several industrial purposes. In this paper, the main goal was to analyze the surface microtexture of Amazon *Anacardium occidentale* L. using multifractal theory. AFM images were used to evaluate the multifractal spatial surface patterns of the adaxial and abaxial sides of the leaf. The 3D maps revealed that the abaxial side is dominated by stomach cells, while striated structures were observed on the adaxial side. The surface of the abaxial side is rougher than the adaxial side. The autocorrelation function calculations showed that the abaxial side has an isotropic surface compared to the adaxial side. Despite this, Minkowski functionals demonstrated that the morphological spatial patterns have robust statistical similarity. Both sides exhibit multifractal behavior, which was verified by the trend observed in the mass exponent and generalized dimension. However, the adaxial side exhibits stronger multifractality and increased vertical complexity compared to the abaxial side. Our findings show that the multifractal spatial patterns of the leaf surface depend on the rough dynamics of the topographic profile. The identification of the multifractal patterns of the structures present on the surface of plant leaves is useful for the fabrication of leaf-architecture-based materials.

Keywords: *Anacardium occidentale*; AFM; Minkowski functionals; multifractality; roughness

check for updates

Citation: Ramos, G.Q.; Matos, R.S.; Das, A.; Kumar, S.; Ţălu, Ş.; da Fonseca Filho, H.D. Correlating Morphology and Multifractal Spatial Patterns of the Leaf Surface Architecture of *Anacardium occidentale* L. *Fractal Fract.* **2022**, *6*, 320. https://doi.org/10.3390/fractalfract6060320

Academic Editor: Jocelyn Sabatier

Received: 27 April 2022
Accepted: 2 June 2022
Published: 7 June 2022

1. Introduction

Fractal structures present on the surface of different types of sample have enormous potential in the elucidation of numerous properties, which has attracted the attention of researchers worldwide in different areas of knowledge. Mandelbrot, who was one of the first to note that nature is generally fractal, used the term fractal for geometric structures with features of all length scales [1]. Currently, atomic force microscopy (AFM), a technique for obtaining images of sample surfaces, is used to identify characteristic patterns, including those in biological samples [2]. Several morphological parameters that can help in the evaluation of the structures of biological surfaces, such as leaves, for example, can be obtained with the AFM technique. The advanced topographical parameters that an AFM image provides can help one to understand various aspects of the physical properties of the surface, such as roughness, flatness, texture symmetry, rough peak density and shape, and texture direction. Several recent works in the literature reported the use of these parameters for the study of different types of biological surface, such as biofilms [3,4], leaves [5], insect structures [6,7], and teeth [8]. Interestingly, researchers have used fractal theory to investigate the surface morphology using 3D AFM maps, for example, [9–12]. However, fractal analysis alone is not able to fully provide the dynamics of a surface. This type of information can be easily accessed by multifractal analysis.

The cashew tree, more precisely *Anacardium occidentale* L., is widely distributed in the Amazon rainforest and belongs to the family *Anacardiaceae* [13,14], a strategic plant, the derivatives of which, such as the chestnut, have a great market value. Furthermore, some biological properties have been extensively studied, such as antioxidant and antibacterial activities [15,16]. Plant leaf wetting is essential for a variety of biological processes, such as seed germination and fungal and bacterial reproduction, as it is essential for water absorption from the soil [17]. Even with the efficiency and effectiveness of pesticide spray applications, leaf wettability and morphology are associated with maximizing the retention and distribution of spray droplets on targeted leaves while minimizing spray solution losses due to droplet bounce [18]. The plant epidermis is usually a hydrophobic material due to the presence of epidermal wax (3D wax crystals on the surface of plants) or, in some cases, a superhydrophobic material, as in the lotus leaf (*Nelumbo nucifera*), where epidermal cells form papillae that create a rough microstructure. Overlying these papillae is a very dense layer of wax crystals called hair-like structures or nanostructural roughness, but structural and chemical modifications cause changes in the surface wetting [19]. The architecture of this layer has been used in the fabrication of materials for different purposes, e.g., scaffolds [20] and polymers [21]. In addition to the stratum corneum wax, the structure of the cells, the presence of hair and the fine structure of the surface, and the folds of the stratum corneum, etc., have a great influence on the wettability of the surface. Thus, the morphology and fractal spatial patterns of the outermost leaf surface (cell shape, size, and fine structure) have a major impact on several functional approaches to the plant boundary layer.

The main objective of this study was to investigate and identify the quantitative and qualitative characteristics of the cashew leaf surface on both sides of the leaf using a powerful tool, that is, multifractal analysis. With the help of the three-dimensionality of the leaf spatial patterns produced by atomic force microscopy (AFM), it is possible to detect differences in the leaf morphology, as it can identify changes in the spatial patterns of nanoscale surfaces [22]. Here, we also analyze the surface texture by multifractal analysis, in addition to studying Minkowski functionals and autocorrelation functions, which, to the best of our knowledge, has never been reported for this plant species.

2. Materials and Methods

2.1. Leaves Obtention

For the study, leaves were collected from a cashew tree on the campus of the Federal University of Amapá in northern Brazil, near French Guiana. To remove dirt particles, each side of the selected sheet was thoroughly washed under running water for 30 s. Then, they were rinsed with deionized water to remove any residual debris that the tap water may have left behind. Leaf samples were deposited at the Herbário Amapaense of the IEPA (Instituto de Pesquisas Científicas e Tecnológicas do Estado do Amapá, Brazil) for proper species identification.

The cashew leaf surface was initially observed on an Olympus Microscope, model Bx40. For this analysis, the leaves, after the collection and washing, were visualized directly on the equipment with no preparation of histological slides.

2.2. AFM Analysis

For AFM scanning, an AFM device (Nanosurf EasyScan 2, ST Instruments, Liefstal, Switzerland) mounted on a Table Stable LDT1 TS-150 platform was used. The device was protected with a sound enclosure to avoid any vibrational influence during the scanning. A silicone tip with a spring constant of 48 N/m and an aluminum-coated cantilever

(Tap190AL-G, from BudgetSensorsTM, Sofia, Bulgaria) were used to generate topographic information of the leaf surface. A small sample of fresh cashew leaves was lightly secured to the sample holder using double-sided tape prior to the measurement. Images were recorded in air at room temperature (296 ± 1 K) and 60 ± 1% relative humidity, generating a scan area of 50 μm × 50 μm in tapping mode with a scan rate of 1 Hz and a resolution of 256 pixels × 256 pixels. Micrographs were analyzed using Gwyddion 2.56 software (Czech Metrology Institute, Brno, Czech Republic) [23] according to ISO 25178-2(2012) [24,25].

2.2.1. Interface Width and Average Roughness

To evaluate the uniformity of the leaf surface on both sides, the AFM images were subjected to calculations of standard one-dimensional statistical parameters, which were the interface width (w), the average roughness (R_a), and the height of ten points (R_z), i.e., the mean absolute value of the five highest peaks and the five lowest valleys along the assessment length. All these parameters were obtained according to ISO 25178-2(2012) [25] using the equations below:

$$w = \frac{1}{N}\sqrt{\sum_{i,j=1}^{N} \left(h(i,j) - \langle h(i,j)\rangle\right)^2} \tag{1}$$

$$R_a = \frac{1}{N^2}\sqrt{\sum_{i,j=1}^{N} |h(i,j) - \langle h(i,j)\rangle|} \tag{2}$$

where $h(i, j)$ is the surface height measured by the AFM at the point (i, j), and $<h(i, j)>$ is the overall average over a total number of $N \times N$ points.

2.2.2. Autocorrelation Function

The autocorrelation function (ACF), being a second-order quantity, is one of the main statistical methods for characterizing AFM images. As it represents the mutual relationship between two points on the surface, it can be expressed as follows:

$$G(\tau_x, \tau_y) = \int\int_{-\infty}^{+\infty} z_1 z_2 w(z_1, z_2, S_x, S_y) dz_1 dz_2 = \lim_{S\to\infty} \frac{1}{S} \iint_S \xi(x_1, y_1)\xi(S_x + x_1, S_y + y_1) dx_1 dy_1 \tag{3}$$

where z_1 and z_2 are the heights at points (x_1, y_1) and (x_2, y_2), respectively, $S_x = x_1 - x_2$, and $S_y = y_1 - y_2$. The function $w(z_1, z_2, S_x, S_y)$ indicates the 2D probability density of the random function $\xi(x, y)$ corresponding to points (x_1, y_1) and (x_2, y_2) and the distance S between these points [26]. The anisotropy ratio (S_{tr}) is defined as the ratio of extreme lateral correlation lengths S_{a1} and S_{a2}, respectively, and is able to indicate directional heterogeneities of the surface [27]:

$$S_{tr} = \frac{S_{a1}}{S_{a2}} \tag{4}$$

Here, S_{a1} and S_{a2} are the fastest and the slowest autocorrelation decays, respectively.

2.2.3. Minkowski Functionals

Minkowski functionals (MFs) are parameters capable of illustrating changes in the spatial structure as a function of time and local geometric and morphological spatial structures [28]. In this work, they were computed by the Gwyddion 2.56 software [23]. MFs can be written as:

$$V = \frac{N_{white}}{N} \tag{5}$$

$$S = \frac{N_{bound}}{N} \tag{6}$$

$$\chi = \frac{C_{white} - C_{black}}{N} \tag{7}$$

where N_{white} is the number of '*white*' pixels, that is pixels above the threshold, N is the total number of pixels, N_{bound} is the number of white–black pixel boundaries, and C_{white} and C_{black} are the number of continuous sets of white and black pixels, respectively.

2.2.4. Multifractal Analysis

A multifractal system that is composed of infinite, interconnected subsets with different fractal dimensions can be characterized when its surface contains $N(\varepsilon)$ square cells. Therefore, the statistical sum is [29,30]:

$$Z(q,\varepsilon) = \sum_{i=1}^{N(\varepsilon)} p_i^q(\varepsilon) \sim \varepsilon^{\tau(q)} \tag{8}$$

where $p_i(\varepsilon) = {r_i(\varepsilon)}/{\sum_{k=1}^{N(\varepsilon)} r_k(\varepsilon)}$, and the power exponent $q \in (-\infty; +\infty)$, with side ε and $r_i(\varepsilon) = \sum Z_{kl}$, is the cumulative fluctuation of the height around the mean value in the i-th square.

D_q (generalized fractal dimension) can be expressed as a function of the mass exponent $\tau(q)$ of the qth order, and q is the order moment using the equation below [31]:

$$D_q = \frac{\tau(q)}{(q-1)} \tag{9}$$

According to Ţălu (2015), the multifractal spectrum function is [31]:

$$f(a(q)) = qa(q) - \tau(q) \tag{10}$$

where $\alpha(q) = d\tau(q)/dq$. D_q and $\alpha(q)$ are calculated as the generalized dimension of Hölder exponents of q, and $f(\alpha)$ refers to the singularity spectrum [32,33].

2.3. Statistical Analysis

It is important to highlight that every experiment presented in this work was carried out on three different leaves, which was necessary for biological replication. In this way, it was possible to analyze the surface variability in different leaves, generating a standard deviation of the results. Three images were taken of each leaf in random regions of each surface on the adaxial and abaxial sides. Statistical data were obtained using OriginPro® software version 9.0 (OriginLab Corporation, Northampton, MA, USA). In all cases, analysis of variance (ANOVA) was applied with a p-value of 0.05.

3. Results and Discussion

3.1. Morphology Analysis

Macroscopic analysis of the leaf revealed that the upper face is dark green, and the lower face is light green, as shown in the photos in Figure 1a,b. The leaf has an obovate shape, pinnate veins, a symmetrical base and obtuse apex, an entire margin, and a smooth surface with straight petioles. Its length is around 15 cm long, and its width is 8 cm. Leaf surfaces, examined by light microscopy, showed an epidermal wall with sinuous cells on both sides (Figure 1c,d). On the adaxial surface, the epidermal cells have a polyhedral shape of irregular size without the presence of stomata. However, in the epidermis of the abaxial surface, stomata were noted. The leaf is of the hypostomatic type, whereas the stomata are of the paracytic type, with random distribution, presenting an ellipsoidal shape. A more complete and detailed analysis can be found elsewhere [13,34].

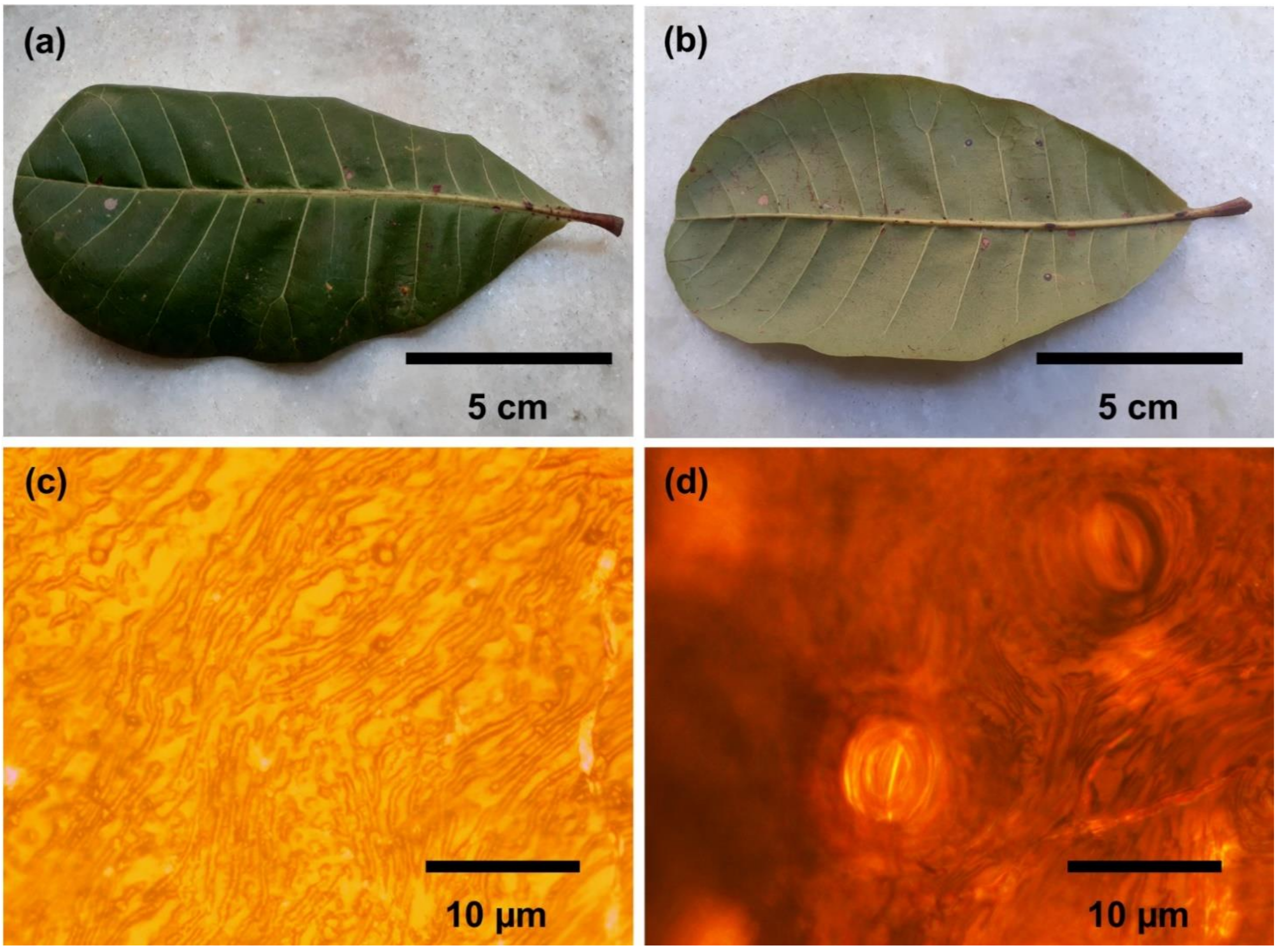

Figure 1. Leaf photographs of *A. occidentale*. (**a**) Adaxial face. (**b**) Abaxial face. Light micrographs at 50× magnification. (**c**) Adaxial and (**d**) abaxial epidermis.

AFM plays a significant role in probing the surface of biological samples [35,36]. In recent times, the relevant aspects of surface topography have been studied from AFM images using stereometric, fractal, and multifractal analysis [37–39]. We can cite the works of Ramos et al. [40,41], where the relevant morphological parameters obtained through AFM images of the adaxial and abaxial surfaces of the cashew leaf were discussed in detail. They showed that the advanced stereometric parameters obtained by the topographic maps of AFM revealed that the two sides have some singularities due to their different morphologies and roughness but similar microtextures. In addition, the results of the fractal analysis showed that the adaxial and abaxial sides have strong microtexture homogeneity, but the adaxial side presented higher surface entropy.

The most pertinent AFM micrographs of the analyzed abaxial and adaxial leaf surfaces of *A. occidentale* are shown in Figure 2, and the corresponding height parameters are displayed in Table 1. A striated cuticular surface was evident for both surface parts, while only the abaxial surface was observed to possess stomata with corrugated cuticles near them. This observation may be related to the adaptation behavior of cashew leaves in response to ecological conditions. Moreover, the quantitative difference between both sides of the leaf surface can be seen in Table 1. The adaxial side displayed an enhanced surface roughness compared to the abaxial side, as manifested by the interface width (w) and average roughness (Sa) values. The results support the enhanced cuticular structure of the adaxial side and can be attributed to the coverage of the surface by microcrystalline wax composed of primary alcohols. On the other hand, the presence of stomata with rippled cuticles contributes to the roughening behavior of the abaxial side [13].

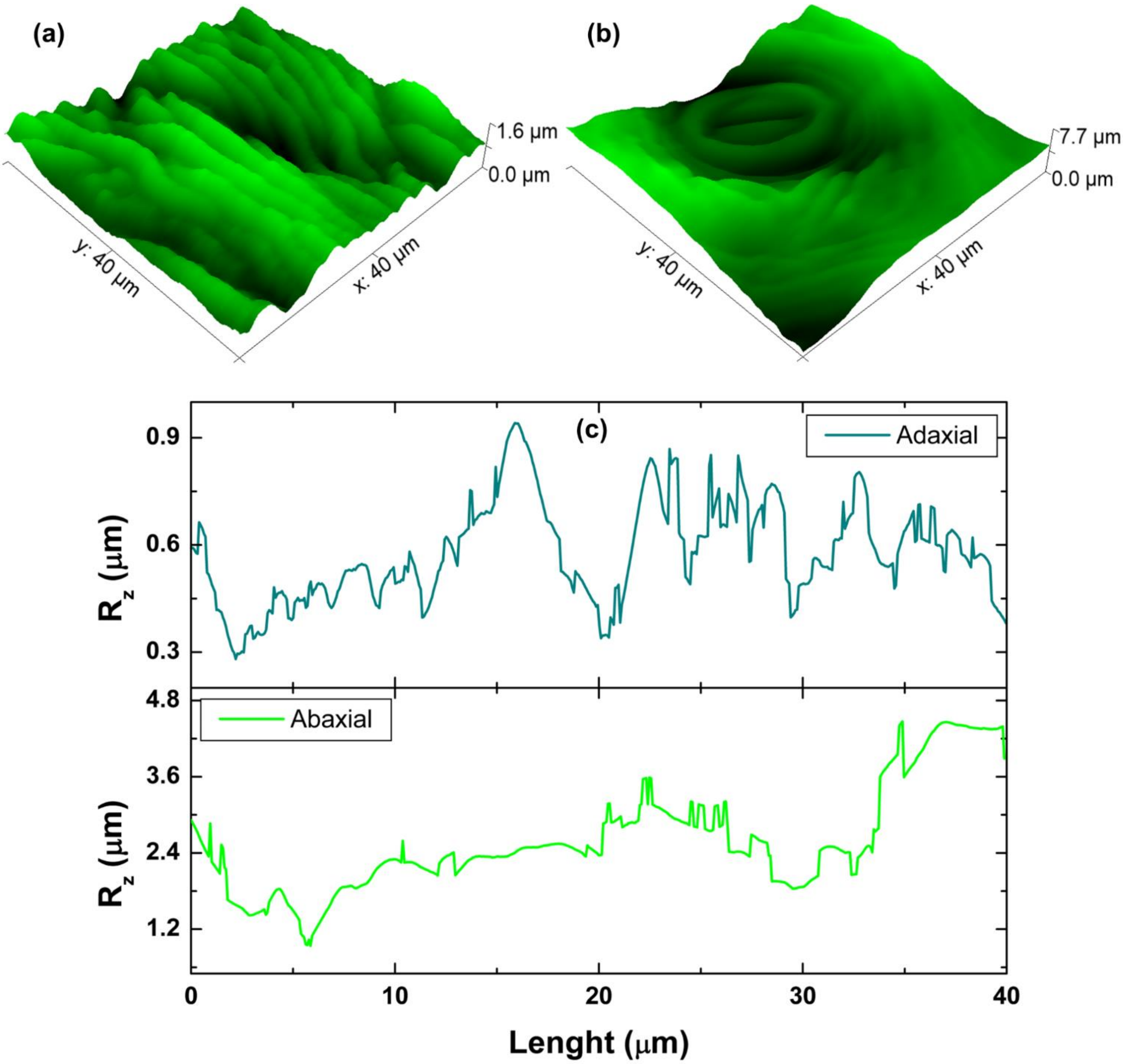

Figure 2. 3D AFM micrographs of (**a**) adaxial and (**b**) abaxial leaf surfaces. (**c**) Ten-point height profiles of both sides of leaf surface as a function of the sample length I, respectively.

Table 1. Relevant roughness and height parameters for the abaxial and adaxial leaf surface from AFM images.

Parameter	Unit	Abaxial	Adaxial
w	[µm]	0.528 ± 0.232	1.352 ± 0.221
R_a	[µm]	0.434 ± 0.189	1.088 ± 0.177
S_p	[µm]	1.451 ± 0.833	4.051 ± 0.786
S_v	[µm]	1.485 ± 0.701	3.190 ± 0.516
S_z	[µm]	2.936 ± 1.499	7.240 ± 1.085

The ten-point height (Sz) computed from the arithmetic sum of maximum peak (S_p) and pit (Sv) heights also displayed a larger value for the adaxial side, indicating a surface with augmented peaks and valleys compared to the abaxial side. This observation contradicts our earlier reported work and can be attributed to the change in the surface morphology in response to the change in environmental conditions, such as humidity and temperature, which affect the efficient adsorption of water [42,43].

3.2. Autocorrelation Function

In recent times, stereometric analysis has had a profound impact on analyzing and understanding the complex three-dimensional (3D) surface characteristics, i.e., microtexture and roughness, and their correlation to the interfacial properties [44,45]. In this regard, the autocorrelation function is utilized to investigate the periodicity or isotropy in an analyzed surface [24]. In other words, it signifies the repeatability of patterns in a surface. Figure 3 shows the trend of the slowest and fastest decay of the normalized autocorrelation function (ACF) corresponding to the studied surfaces, and their corresponding values are given in Table 2.

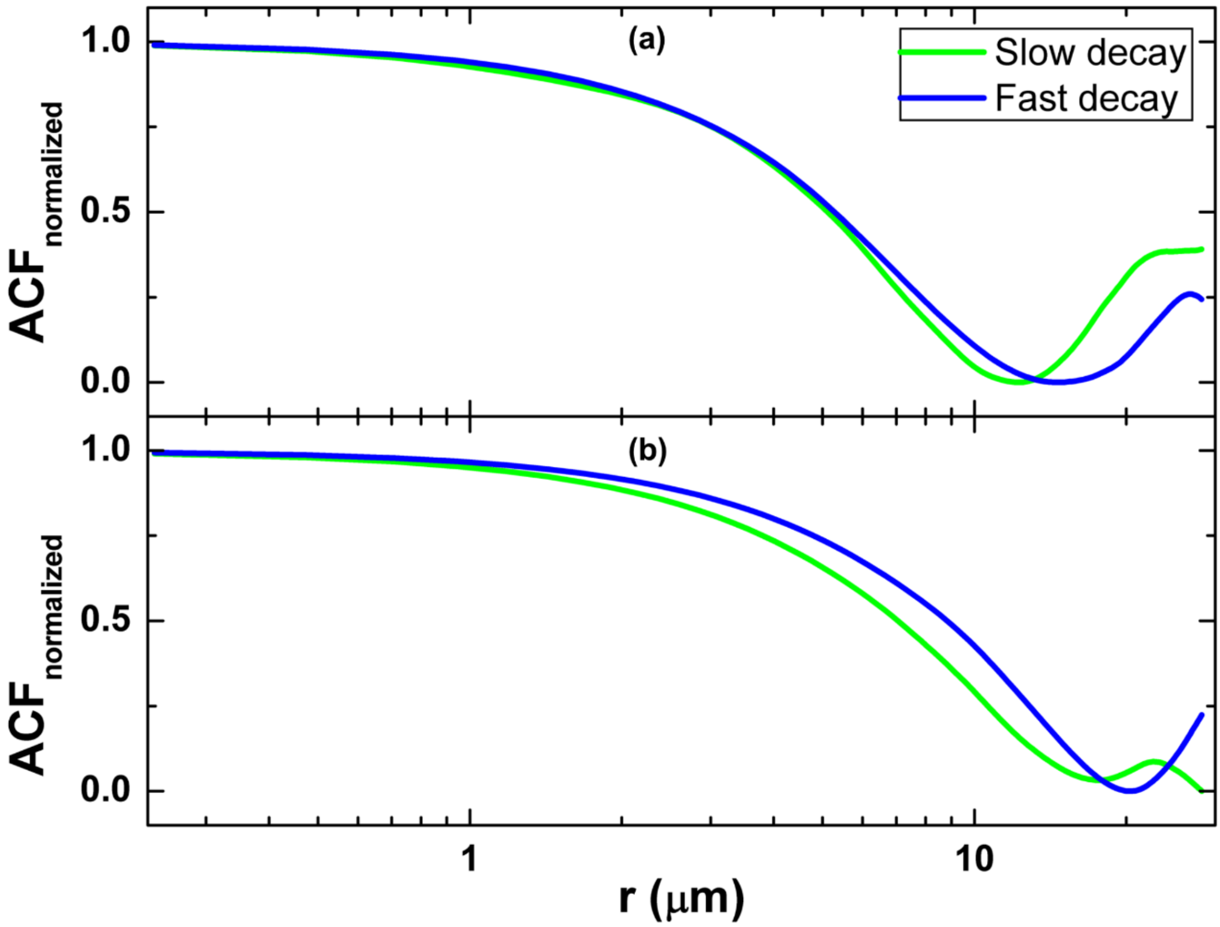

Figure 3. The autocorrelation functions (ACFs) of (**a**) abaxial and (**b**) adaxial leaf surface as a function of the sample length (r).

Table 2. The fastest (τ_{a1}) and the slowest (τ_{a2}) decay directions, decay length (S_{a1} and S_{a2}), and anisotropy factor (S_{tr}) for the investigated samples.

Parameter	Unit	Abaxial	Adaxial
τ_{a1}	[°]	31.08	15.70
τ_{a2}	[°]	−89.17	−72.92
S_{a1}	[nm]	6.435	6.202
S_{a2}	[nm]	8.091	20.86
S_{tr}	[nm]	0.7953	0.2973

The exponentially decreasing behavior of the ACF was evident for both surfaces and indicated the presence of self-affine properties in the leaf surfaces. In addition, the apparent oscillatory behavior of the ACF for the adaxial surface supported the argument of increased roughness [46,47]. It is important to note that the abaxial surface displayed a larger value for the fastest decay of ACF, also known as the autocorrelation length. According to Davim, smaller autocorrelation length values are ascribed to closed surfaces, while large values are associated with opened surfaces [48]. This suggests the existence of a positive correlation between surface heights. Furthermore, larger values of the slowest decay length for the adaxial part suggest a steep difference between surface heights, whereas a small difference between them can bring an apparent change in the surface roughness. An identical feature shared between the surface microtexture and the ACF is the texture aspect ratio (S_{tr}). It is defined as the ratio between the fastest and slowest decay of the ACF in the horizontal direction and ranges from 0 to 1, where a completely anisotropic surface is characterized by $Str = 0$ [25]. In this framework, the value $S_{tr} \sim 1$ for the abaxial side indicated isotropic behavior, i.e., the absence of a dominant texture direction. The analysis indicated the possibility of measuring properties like wettability across the lower surface of cashew leaves. The stereometric analysis validated the qualitative information, as seen in Figure 2, and shed light on the difference in the microtexture of both sides of the analyzed leaf surface.

3.3. Minkowski Functionals

The morphology of a surface following a random probability distribution is studied using the Minkowski functionals. These parameters are computed based on separating the AFM images into high and low parts, by thresholding, where the high and low regions represent plateaus and valleys [49], respectively. Therefore, the plots of the Minkowski volume, boundary, and connectivity as a function of the threshold (z) are shown in Figure 4, and their corresponding values are presented in Table 3. The presence of a greater density of peaks in the upper side was apparent with a value >0.5 for the Minkowski volume, although the ANOVA suggested a similar topography without a significant difference between both leaf surfaces. In addition, a symmetrical functional with greater surface coverage for the abaxial side is visible in Figure 4a. Moreover, a significant degree of similarity in the surface morphology of the analyzed samples was reflected from the Minkowski boundary values, as seen in Figure 4b. According to Mwema et al., Minkowski connectivity is a measure of the difference in the number of white- and black-level regions and describes the present fractal pattern as evident from the self-affine behavior of the surface morphologies [50]. Its largest value, computed from Figure 4c using the Gaussian radially averaged power spectral density function, exhibited larger values for the adaxial surface, suggesting the presence of significant peaks compared to trenches and valleys and, thus, explaining the observed roughening trend in the samples.

3.4. Multifractal Analysis

The multifractal analysis of the upper and lower side of the cashew leaf was performed to probe the minute details in the growth probabilities of surface heights which may arise due to the local irregularities in the randomly growing surface heights. The nonlinear behavior of the mass exponent $\tau(q)$ with moment of order (q), as shown in Figure 5a, signified the presence of a multifractal behavior in the abaxial and adaxial part of the leaf surface. In addition, the nonlinear, decreasing nature of the generalized dimension (D_q) as a function of (q) in Figure 5b established the multifractal nature of the analyzed surfaces [51]. The left-hooked multifractal spectra corresponding to the adaxial and abaxial leaf surfaces are shown in Figure 5c. The corresponding values are given in Table 4. According to Yadav et al. [47], the maximum and minimum surface height probabilities representing the most and least singularities are denoted by α_{min} and α_{max}, respectively.

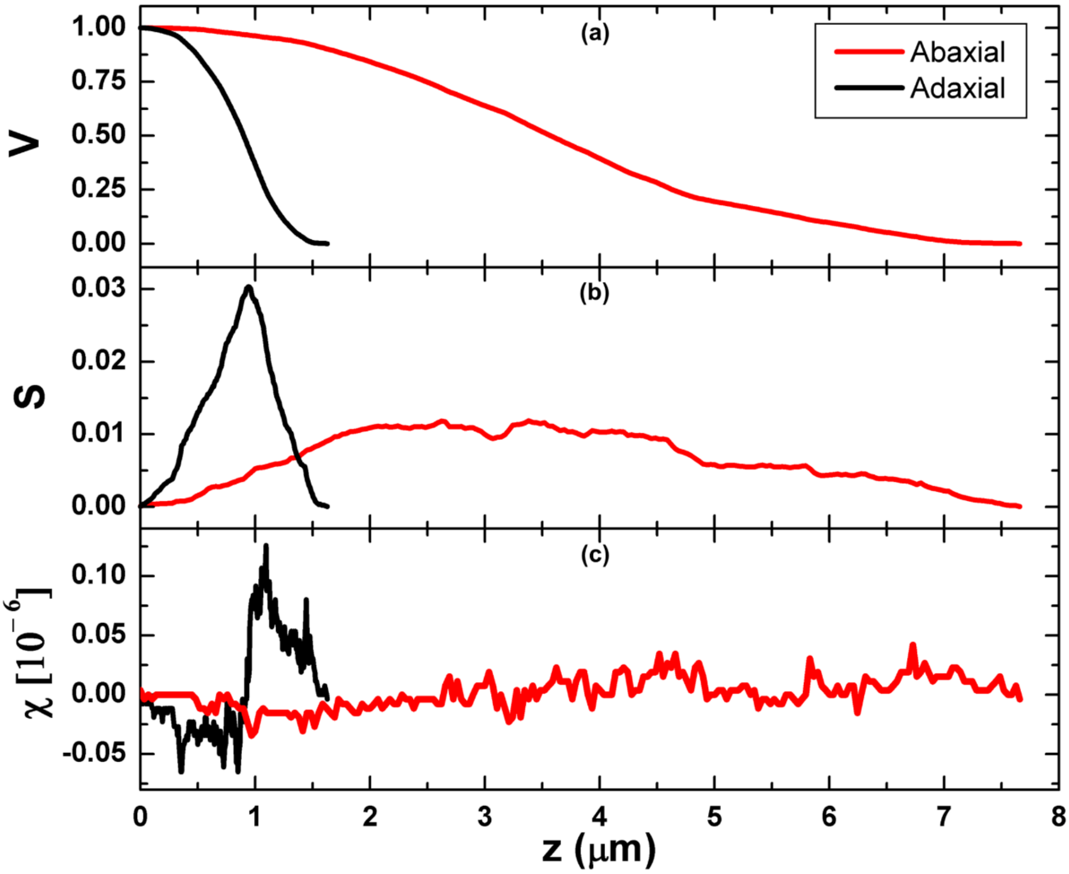

Figure 4. The MFs of AFM images of abaxial and adaxial leaf surface for (**a**) Minkowski volume, (**b**) Minkowski boundary, and (**c**) Minkowski connectivity.

Table 3. Minkowski measures computed from Figure 3.

Parameter	Unit	Abaxial	Adaxial
V *	[–]	0.485 ± 0.090	0.514 ± 0.073
S [10^{-3}] *	[–]	2.263 ± 1.819	2.694 ± 1.808
χ [10^{-6}] *	[–]	6.283 ± 1.205	7.951 ± 2.650

* Samples without significant difference, ANOVA one-way ($p < 0.05$).

In this regard, the multifractal spectrum width computed from $\Delta\alpha = \alpha_{max} - \alpha_{min}$ signifies the range of growth probabilities in a surface and the strength of multifractality. In this context, the weak multifractal nature of the abaxial surface compared to the adaxial side was observed, as seen in Table 4. However, by analyzing the curves of Figure 5c, it is possible to clearly see that the abaxial surface had a greater singularity (because it had the highest singularity strength [52] when compared with the adaxial surface). In addition, an enhanced degree of surface complexities, which can be attributed to the non-uniform distribution of surface heights, was present in the upper part of the leaf surface. Furthermore, the difference in fractal dimension $\Delta f = f(\alpha_{max}) - f(\alpha_{min})$ displayed a smaller value for the abaxial side, suggesting the presence of denser regions compared to unsubstantial sites, along with reduced complexity in the vertical direction which validated the smoothening trend on this part of the leaf surface [37]. The observation from multifractal analysis validated and added to the information gained from stereometric and Minkowski functionals analysis and, thus, should be considered important for obtaining a deep insight into the roughening and microtexture dynamics and surface complexities in the adaxial and abaxial surfaces of a cashew leaf.

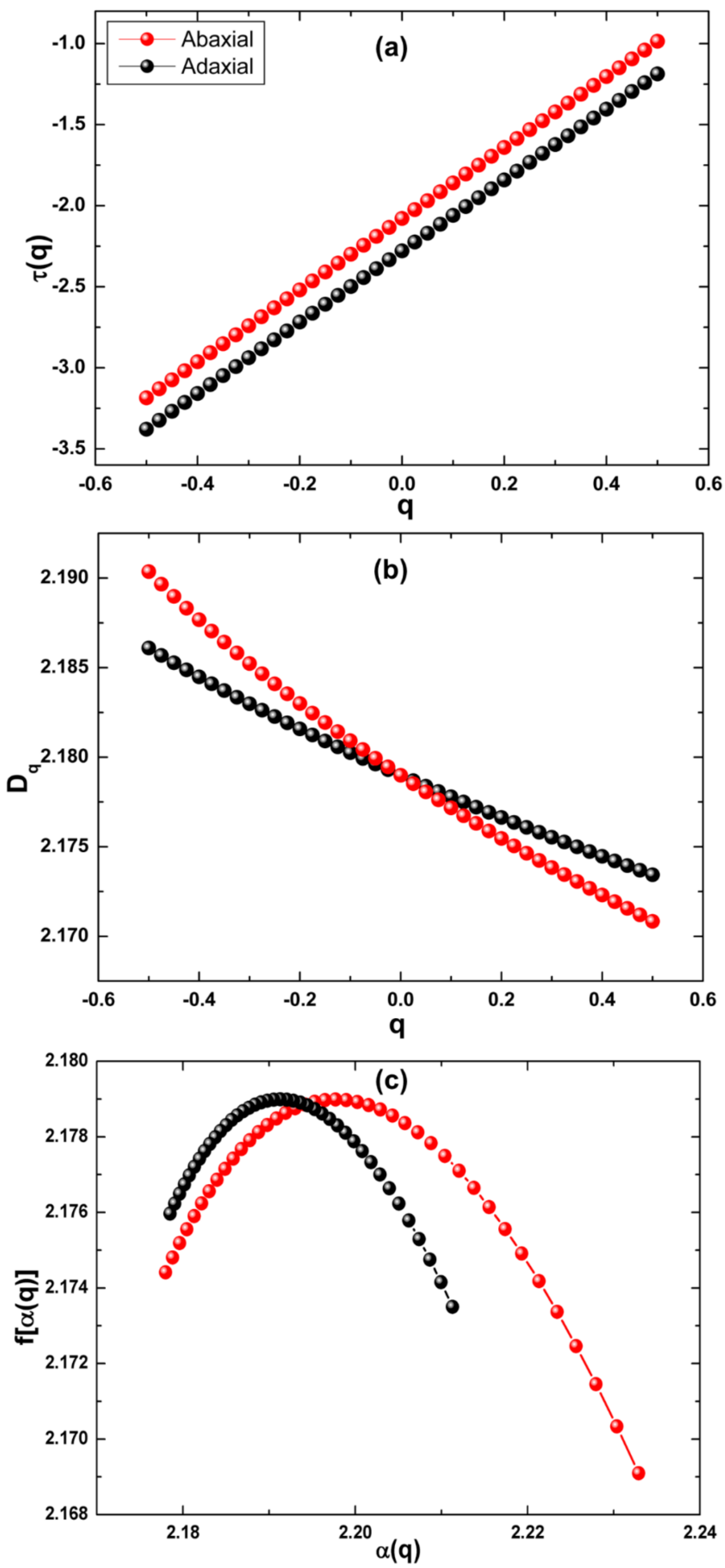

Figure 5. (**a**) Mass exponent $\tau(q)$, (**b**) generalized dimensions D_q, and (**c**) multifractal spectra ($f(\alpha)$ versus α) as a function of the order of moments computed for abaxial and adaxial leaf surfaces. For clarity, the mass exponent curves for abaxial and adaxial were shifted by 0.1 and -0.1, respectively.

Table 4. Measures of multifractal spectra of the cashew leaf surface.

Parameter	Abaxial	Adaxial
α_{max}	2.2112	2.2329
α_{min}	2.1785	2.1779
$\Delta\alpha$	0.0327	0.0550
$f(\alpha_{max})$	2.1735	2.1690
$f(\alpha_{min})$	2.1759	2.1744
Δf	0.0024	0.0054

4. Conclusions

In summary, we studied the roughening dynamics and microtexture of the adaxial and abaxial surfaces of cashew tree leaves using morphological, Minkowski functionals, and multifractal approaches. The heights parameters categorically revealed the presence of enhanced roughness on the adaxial part with significant peak and valley heights. The ACF analysis revealed the positive correlation between surface heights on the abaxial side with an isotropic surface, as suggested by the texture aspect ratio. The significant similarity in the morphology of both analyzed surfaces, along with the greater surface coverage on the lower side of the leaf surface, was observed from the Minkowski boundary and volume calculations. In addition, the Euler–Poincaré characteristic suggested the presence of significant peaks on the adaxial side, validating its augmented surface roughness. The multifractal nature of the analyzed surfaces was probed using multifractal detrended fluctuation analysis. The trend of the mass exponent and generalized dimension with moments validated the multifractal nature of cashew leaf surfaces. The width of the multifractal spectrum and the difference in fractal dimension showed the lowest value for the abaxial side, revealing its weak multifractality and reduced vertical complexity. This work heralds the possibility of obtaining insight into the structure of cashew leaf surfaces for scientific interest, especially for the fabrication of new materials based on their unique leaf architecture and spatial patterns.

Author Contributions: G.Q.R., A.D. and H.D.d.F.F.: conceptualization, methodology, resources, writing—review and editing. G.Q.R. and R.S.M.: sample preparation, data curation, original draft preparation. A.D., S.K. and R.S.M.: writing—review and editing, and supervision. Ș.Ț. and H.D.d.F.F.: conceptualization, methodology, funding acquisition, reviewing. Ș.Ț., R.S.M., S.K. and H.D.d.F.F.: formal analysis, investigation, project administration, and writing—review and editing. All authors have read and agreed to the published version of the manuscript.

Funding: This research was funded by CNPq grant number 442601/2019-0.

Institutional Review Board Statement: Not applicable.

Informed Consent Statement: Not applicable.

Data Availability Statement: The data used to support the findings of this study are available from the corresponding author upon request.

Acknowledgments: The authors thank the use of the infrastructure of the Analytical Center of Universidade Federal do Amazonas (UFAM). We would like to thank the Laboratório de Síntese de Nanomateriais e Nanoscopia (LSNN) associated with the Sistema Nacional de Laboratórios em Nanotecnologias (SisNANO).

Conflicts of Interest: The authors declare no conflict of interest.

References

1. Falconer, K.J. *Fractals: A Very Short Introduction*; Oxford University Press: Oxford, UK, 2013. [CrossRef]
2. Liang, W.; Shi, H.; Yang, X.; Wang, J.; Yang, W.; Zhang, H.; Liu, L. Recent advances in AFM-based biological characterization and applications at multiple levels. *Soft Matter* **2020**, *16*, 8962–8984. [CrossRef]
3. Ahmed, B.; Ameen, F.; Rizvi, A.; Ali, K.; Sonbol, H.; Zaidi, A.; Khan, M.S.; Musarrat, J. Destruction of Cell Topography, Morphology, Membrane, Inhibition of Respiration, Biofilm Formation, and Bioactive Molecule Production by Nanoparticles of Ag, ZnO, CuO, TiO_2, and Al_2O_3 toward Beneficial Soil Bacteria. *ACS Omega* **2020**, *5*, 7861–7876. [CrossRef]

4. Uzoechi, S.C.; Abu-Lail, N.I. Variations in the Morphology, Mechanics and Adhesion of Persister and Resister *E. coli* Cells in Response to Ampicillin: AFM Study. *Antibiotics* **2020**, *9*, 235. [CrossRef] [PubMed]
5. Omar, M.; Salcedo, C.; Ronald, R.; Zamora, M.; Tavares, C. Study fractal leaf surface of the plant species *Copaifera* sp. using the Microscope Atomic-Force-AFM. *Rev. ECIPerú* **2016**, *13*, 10–16. [CrossRef]
6. Sobola, D.; Ţălu, Ș.; Sadovsky, P.; Papez, N.; Grmela, L. Application of AFM Measurement and Fractal Analysis to Study the Surface of Natural Optical Structures. *Adv. Electr. Electron. Eng.* **2017**, *15*, 569–576. [CrossRef]
7. Garczyk, Z.; Stach, S.; Ţălu, Ș.; Sobola, D.; Wróbel, Z. Stereometric Parameters of Butterfly Wings. *J. Biomim. Biomater. Biomed. Eng.* **2017**, *31*, 1–10. [CrossRef]
8. Nezafat, N.B.; Ghoranneviss, M.; Elahi, S.M.; Shafiekhani, A.; Ghorannevis, Z.; Solaymani, S. Topographic characterization of canine teeth using atomic force microscopy images in nano-scale. *Int. Nano Lett.* **2019**, *9*, 311–315. [CrossRef]
9. Bitler, A.; Dover, R.; Shai, Y. Fractal properties of macrophage membrane studied by AFM. *Micron* **2012**, *43*, 1239–1245. [CrossRef] [PubMed]
10. Gao, H.; Qiang, T. Fracture Surface Morphology and Impact Strength of Cellulose/PLA Composites. *Materials* **2017**, *10*, 624. [CrossRef] [PubMed]
11. Xagas, A.; Androulaki, E.; Hiskia, A.; Falaras, P. Preparation, fractal surface morphology and photocatalytic properties of TiO_2 films. *Thin Solid Films* **1999**, *357*, 173–178. [CrossRef]
12. Buzio, R.; Boragno, C.; Valbusa, U. Contact mechanics and friction of fractal surfaces probed by atomic force microscopy. *Wear* **2003**, *254*, 917–923. [CrossRef]
13. Ramos, G.Q.; Cotta, E.A.; Filho, H.D.D.F. Studies on the ultrastructure in *Anacardium occidentale* L. leaves from Amazon in northern Brazil by scanning microscopy. *Scanning* **2016**, *38*, 329–335. [CrossRef] [PubMed]
14. Mabberley, D.J. *Mabberley's Plant-Book*; Cambridge University Press: Cambridge, UK, 2017. [CrossRef]
15. Ifesan, B.O.T. Antioxidant and Antimicrobial Properties of Selected Plant Leaves. *Eur. J. Med. Plants* **2013**, *3*, 465–473. [CrossRef]
16. Baptista, A.; Gonçalves, R.V.; Bressan, J.; Pelúzio, M.D.C.G. Antioxidant and Antimicrobial Activities of Crude Extracts and Fractions of Cashew (*Anacardium occidentale* L.), Cajui *(Anacardium microcarpum)*, and Pequi (*Caryocar brasiliense* C.): A Systematic Review. *Oxidative Med. Cell. Longev.* **2018**, *2018*, 3753562. [CrossRef]
17. McHale, G.; Newton, M.I.; Shirtcliffe, N.J. Water-repellent soil and its relationship to granularity, surface roughness and hydrophobicity: A materials science view. *Eur. J. Soil Sci.* **2005**, *56*, 445–452. [CrossRef]
18. Dong, X.; Zhu, H.; Yang, X. Characterization of droplet impact and deposit formation on leaf surfaces. *Pest Manag. Sci.* **2015**, *71*, 302–308. [CrossRef] [PubMed]
19. Samaha, M.; Tafreshi, H.V.; Gad-El-Hak, M. Superhydrophobic surfaces: From the lotus leaf to the submarine. *Comptes Rendus Mécanique* **2012**, *340*, 18–34. [CrossRef]
20. Periasamy, V.S.; Athinarayanan, J.; Alshatwi, A.A. Bio-inspired plant leaf skeleton based three dimensional scaffold for three dimensional cell culture. *Sustain. Chem. Pharm.* **2020**, *18*, 100321. [CrossRef]
21. Iravani, S.; Varma, R.S. Plants and plant-based polymers as scaffolds for tissue engineering. *Green Chem.* **2019**, *21*, 4839–4867. [CrossRef]
22. da Conceição, W.S.; Ţălu, Ș.; Matos, R.S.; Ramos, G.Q.; Zayas, F.G.; Filho, H.D.D.F. Stereometric characterization of Dinizia excelsa Ducke wood from Amazon rainforest using atomic force microscopy. *Microsc. Res. Tech.* **2021**, *84*, 1431–1441. [CrossRef]
23. Nečas, D.; Klapetek, P. Gwyddion: An open-source software for SPM data analysis. *Open Phys.* **2012**, *10*, 181–188. [CrossRef]
24. Blateyron, F. The Areal Field Parameters. In *Characterisation Areal Surface Texture*; Springer: Berlin/Heidelberg, Germany, 2013; pp. 15–43. [CrossRef]
25. Blateyron, F. *Characterisation of Areal Surface Texture*; Springer: Berlin/Heidelberg, Germany, 2013. [CrossRef]
26. Nečas, D.; Klapetek, P. One-dimensional autocorrelation and power spectrum density functions of irregular regions. *Ultramicroscopy* **2013**, *124*, 13–19. [CrossRef] [PubMed]
27. Dong, W.; Sullivan, P.; Stout, K. Comprehensive study of parameters for characterising three-dimensional surface topography. *Wear* **1994**, *178*, 45–60. [CrossRef]
28. Armstrong, R.T.; McClure, J.E.; Robins, V.; Liu, Z.; Arns, C.H.; Schlüter, S.; Berg, S. Porous Media Characterization Using Minkowski Functionals: Theories, Applications and Future Directions. *Transp. Porous Media* **2019**, *130*, 305–335. [CrossRef]
29. Astinchap, B.; Ghanbaripour, H.; Amuzgar, R. Multifractal study of TiO2 thin films deposited by MO-CVD method: The role of precursor amount and substrate temperature. *Optik (Stuttg)* **2020**, *222*, 165384. [CrossRef]
30. Qiu, L.; Song, D.; He, X.; Wang, E.; Li, Z.; Yin, S.; Wei, M.; Liu, Y. Multifractal of Electromagnetic Waveform and Spectrum about Coal Rock Samples Subjected to Uniaxial Compression. *Fractals* **2020**, *28*, 2050061. [CrossRef]
31. Fu, C.; Lu, F.; Zhang, G. Discrimination Analysis of Coal and Gangue Using Multifractal Properties of Optical Texture. *Int. J. Coal Prep. Util.* **2020**, *40*, 1–13. [CrossRef]
32. Gao, Y.; Gu, Y.; Mu, S.; Jiang, J.; Liu, J. The multifractal property of heterogeneous microstructure in cement paste. *Fractals* **2021**, *29*, 2140006. [CrossRef]
33. Ju, X.; Jia, Y.; Li, T.; Gao, L.; Gan, M. Morphology and multifractal characteristics of soil pores and their functional implication. *Catena* **2021**, *196*, 104822. [CrossRef]
34. Ramos, G.Q.; Da Fonseca De Albuquerque, M.D.; Ferreira, J.L.P.; Cotta, E.A.; Da Fonseca Filho, H.D. Molhabilidade e morfologia da superfície da folha em cajueiro da Amazônia na Região Norte do Brasil. *Acta Sci. Biol. Sci.* **2016**, *38*, 215–220. [CrossRef]

35. Müller, D.J.; Helenius, J.; Alsteens, D.; Dufrêne, Y. Force probing surfaces of living cells to molecular resolution. *Nat. Chem. Biol.* **2009**, *5*, 383–390. [CrossRef] [PubMed]
36. Muller, D.J. AFM: A Nanotool in Membrane Biology. *Biochemistry* **2008**, *47*, 7986–7998. [CrossRef] [PubMed]
37. Modabberasl, A.; Sharifi, M.; Shahbazi, F.; Kameli, P. Multifractal analysis of DLC thin films deposited by pulsed laser deposition. *Appl. Surf. Sci.* **2019**, *479*, 639–645. [CrossRef]
38. Ghosh, K.; Pandey, R.K. Assessment of fractal and multifractal features of sol-gel spin coated ZnO thin film surface. *Mater. Res. Express* **2019**, *6*, 086454. [CrossRef]
39. Ghosh, K.; Pandey, R.K. Fractal and multifractal analysis of In-doped ZnO thin films deposited on glass, ITO, and silicon substrates. *Appl. Phys. A* **2019**, *125*, 98. [CrossRef]
40. Ramos, G.Q.; Matos, R.S.; Filho, H.D.D.F. Advanced Microtexture Study of *Anacardium occidentale* L. Leaf Surface From the Amazon by Fractal Theory. *Microsc. Microanal.* **2020**, *26*, 989–996. [CrossRef] [PubMed]
41. Ramos, G.Q.; Da Costa, C.; Da Costa, M.E.H.M.; Pinto, E.P.; Matos, R.S.; Filho, H.D.D.F. Stereometric analysis of Amazon rainforest Anacardium occidentale L. leaves. *Planta* **2021**, *253*, 6. [CrossRef] [PubMed]
42. Woodward, F.I.; Kelly, C.K. The influence of CO2 concentration on stomatal density. *New Phytol.* **1995**, *131*, 311–327. [CrossRef]
43. Koren, I.; Kaufman, Y.J.; Washington, R.; Todd, M.C.; Rudich, Y.; Martins, J.V.; Rosenfeld, D. The Bodélé depression: A single spot in the Sahara that provides most of the mineral dust to the Amazon forest. *Environ. Res. Lett.* **2006**, *1*, 014005. [CrossRef]
44. Das, A.; Matos, R.S.; Pinto, E.P.; Yadav, R.P.; Ţălu, Ș.; Kumar, S. 3D micromorphology-contact resistance-conductivity insights of quasi 2D Cd1-xPbxS thin films: Investigation based on stereometric and fractal analysis. *Mater. Chem. Phys.* **2022**, *278*, 125635. [CrossRef]
45. Maity, G.; Yadav, R.P.; Ojha, S.; Singhal, R.; Kanjilal, D.; Patel, S.P. Micro-morphological investigations on wettability of Al-incorporated c -Si thin films using statistical surface roughness parameters. *Surf. Interface Anal.* **2022**, *54*, 174–186. [CrossRef]
46. Das, A.; Yadav, R.P.; Chawla, V.; Kumar, S.; Ţălu, Ș.; Pinto, E.P.; Matos, R.S. Analyzing the surface dynamics of titanium thin films using fractal and multifractal geometry. *Mater. Today Commun.* **2021**, *27*, 102385. [CrossRef]
47. Yadav, R.P.; Dwivedi, S.; Mittal, A.; Kumar, M.; Pandey, A. Fractal and multifractal analysis of LiF thin film surface. *Appl. Surf. Sci.* **2012**, *261*, 547–553. [CrossRef]
48. Davim, J.P. *Tribology for Engineers: A Practical Guide*; Elsevier: Amsterdam, The Netherlands, 2011; p. 296.
49. Salerno, M.; Banzato, M. Minkowski Measures for Image Analysis in Scanning Probe Microscopy. *Microsc. Anal.* **2005**, *19*, 13–15.
50. Mwema, F.M.; Akinlabi, E.T.; Oladijo, O.P. Effect of Substrate Type on the Fractal Characteristics of AFM Images of Sputtered Aluminium Thin Films. *Mater. Sci.* **2019**, *26*, 49–57. [CrossRef]
51. Ghosh, K.; Pandey, R. Annealing time induced roughening in ZnO thin films: A fractal and multifractal assessment. *Mater. Sci. Semicond. Process.* **2020**, *106*, 104771. [CrossRef]
52. Liu, C.; Jiang, X.-L.; Liu, T.; Zhao, L.; Zhou, W.-X.; Yuan, W.-K. Multifractal analysis of the fracture surfaces of foamed polypropylene/polyethylene blends. *Appl. Surf. Sci.* **2009**, *255*, 4239–4245. [CrossRef]